



# Impact of shock waves on morphological, structural, optical and dielectric properties of L-alaninium maleate crystals

M. Deepa<sup>1</sup>, S. Sahaya Jude Dhas<sup>2</sup>, S. A. Martin Britto Dhas<sup>1,a)</sup>

<sup>1</sup> Shock Wave Research Laboratory, Department of Physics, Abdul Kalam Research Center, Sacred Heart College, Tirupattur, Tamil Nadu 635 601, India

<sup>2</sup> Department of Physics, Kings Engineering College, Sriperumbudur, Chennai, Tamil Nadu 602 117, India

<sup>a)</sup> Address all correspondence to this author. e-mail: martinbritto@shcpt.edu

Received: 12 January 2023; accepted: 11 August 2023; published online: 5 September 2023

Single crystals of L-alaninium maleate (LAM) were successfully grown by utilizing the Sankaranarayanan–Ramasamy (SR) method. The cut and polished crystal of LAM was subjected to shock waves of 1.7 Mach number. The dynamic shock wave impact on the test crystal in terms of morphological, structural, optical, and dielectric properties was analyzed using optical microscope, powder X-ray diffractometer, UV–Visible spectrometer, and impedance analyzer, respectively. From the observed data under shock-loaded conditions, LAM crystal exhibits a good structural stability against shock waves. The obtained values of optical transmittance of the test crystal for different number of shock pulses show that there is a slight reduction of transmission because of the induced defects and deformations formed under shocked conditions. From the dielectric study, it is observed that the values of dielectric constant and dielectric loss are reduced substantially under shock-loaded conditions.

## Introduction

Materials treated with shock waves have the potential to progressively outpace the impending constraints that exist in functional materials while on the path of identifying the apt materials for specified applications. It could be accomplished with the process of accessing the impact of aftershocks on materials in terms of their properties such that it may unlock the mystery of identifying a range of possible stable materials that were previously inaccessible to several other methods such as static pressure compression and irradiation methods. Shock wave research, which was established many years ago, had been initiated primarily for the applications in aerospace whereas it has extended its influence in such a way that there are many applications which keep emerging now in fields such as geology, medical, materials science, etc. Materials of good structural stability against shock waves can have the prominence of being used in devices which have to be in an environment that is highly fluctuating. On those lines, crystalline amino acids are the interesting and important molecular materials to be tested under shocked conditions as they are generally by and large stable. Amino acids form salts easily with many carboxylic acids such that they have

many functional groups which are involved in more of hydrogen bonds compared to its pure form. Hydrogen-bonded materials attract the researchers with more attention since minute changes in hydrogen bonds can lead to major changes in the material whereby either it will induce changes in properties such as structural, morphological, phase, electrical, magnetic, optical, molecular etc. or it would retain every property withstanding the external stimuli [1]. Glycine shows high polymorphism under high-pressure conditions [2]. The L-cystine has the monoclinic crystal system between 2.5 and 3.9 GPa whereas it is the orthorhombic between 1.1 and 2.5 GP. DL-Cysteine also undergoes high-pressure phase transition between 0.1 and 5 GPa. In contrast bis DL-cysteinium oxalate exhibit no phase transition up to 9.5 GPa [3] whereby it could be noted that adding the second component to the system can prevent the phase transition. On the other hand, DL-alanine shows no high-pressure transition [4], but DL-alaninium semi-oxalate monohydrate exhibits phase transition between 1.5 and 2.4 GPa. In this case, homomolecular framework is broken under high pressure, which leads to phase transition [1]. L-Alanine is a prominent amino acid that possess the zwitterionic nature and form hydrogen bonding in the form

of N-H...O, which is very strong in nature. L-Alanine was the first and the only crystal, to date, among the amino acid materials to be studied extensively under high pressure. At the pressure of 15.46 GPa, L-alanine becomes amorphous in nature, and it is reversible on decreasing the pressure at ambient condition [5]. It is the only amino acid studied at such a high-pressure range and shows amorphous nature. It crystallizes with many carboxylic acids such as L-alaninium maleate (LAM), L-alaninium oxalate etc. LAM is one of the potential molecular crystals that have non-linear optical (NLO) property. The growth and characterization of LAM single crystals of bulk nature have been reported by many researchers for NLO applications [6–15]. So far, to date, no high-pressure studies have been carried out on LAM crystals such that it is important to study the structural behavior of this crystal in those environments since the properties such as optical and electrical are highly structure dependent.

Shock wave recovery experiment on materials is an emerging recent research area which provides information about the materials under extreme conditions of simultaneous high pressure and high temperature [16, 17]. Some materials undergo phase transition during shock loading whereas a few other materials withstand the high pressure and temperature of shock waves. Moreover, a few properties of some materials are tuned by the exposure of shock waves whereas some materials' structural and electrical properties are greatly affected by shock-induced defects. It is possible to explore and identify novel materials that can be tuned with application-oriented properties under shocked conditions. Benzil and copper sulfate crystals exhibit enhancement of optical transmittance by shock-induced dynamic recrystallization, whereas optical transmittance of triglycine sulfate crystal is reduced [18–20]. Potassium dihydrogen phosphate (KDP) crystal shows structural stability against shock waves [21]. The transparency of the sapphire crystal is reduced under shock loads of 100–130 GPa [22]. Mashimo et al. have reported the phase transition in KCl crystals from B1 to B2 structure under shocked and static compression wherein it is found that phase transition along different directions takes place at different temperatures [23]. Hemmi et al. have investigated the shock-induced changes in anthracene crystals with which they have reported a red shift of absorption edge at the pressure range of 6 GPa wherein a red shift is observed due to dimer type defects formed in the crystals by the shock impact [24]. Suren-dra et al. have reported the formation of complex macro-scale structures because of the shock wave processing of simple amino acids [25]. Amino acids such as L-threonine and L-leucine have been reported under shock-loaded conditions [26, 27]. L-Threonine shows three phase transitions under shocked conditions such as  $P_{2_1}2_12_1$  to  $P_{2_1}$  at 3rd shocked condition while becomes amorphous after 5th shocked condition and again  $P_{2_1}$  phase is obtained after 6th shock while  $P_{2_1}2_12_1$  phase reappears after

8th shock. L- $\alpha$  Leucine shows conformational phase changes from phase I to phase II. On these counts, the purpose of the proposed work is to study the structural, optical, and dielectric properties of LAM crystals under shocked conditions.

## Results and discussions

### Surface analysis

Optical microscopy is an effective tool of surface analysis which is used to study and infer the surface damages such as pits and cracks. The surface defects have greater influence over optical transmission through the crystal medium since these defects could act as absorption as well as scattering centers of incoming light. An optical microscope (Weswox) has been utilized in the morphological analysis of the control- and shock-exposed samples. The captured images of the crystal surface before and after shock-loading conditions are presented in Fig. 1.

From the microscopic images, it is apparent that the surface of the control crystal was defect free. Under shock-loaded conditions, defects such as micro-voids and micro-cracks have been formed which is very well reflected on the surface of the test crystal as seen in Fig. 1. After the 1st shock-loaded condition, the surface of the crystal was completely affected because of the shock-induced defects. When the number of shocks has been increased from the 2nd to 3rd shocks, the defect density has reduced in the crystal as it had to undergo the process of shock-induced dynamic recrystallization. Further increasing to 4th shock, cracks have been observed on the surface of the crystal. Interestingly, those cracks have disappeared after the 5th shock, which could be as a result of the typical dynamic recrystallization induced by the impact of shock waves.

There are many reports available in the literature for the dynamic recrystallization induced by shock waves [28, 29]. For the dynamic recrystallization to occur, the condition that is to be satisfied is  $T \geq 0.4 T_m$ , where  $T$  is the temperature associated with the shock waves and  $T_m$  is the melting point of LAM. It is reported that melting point of LAM crystal is 435 K. The crystal is loaded with shock waves of 1.7 Mach number which is associated with the transitory temperature of 644 K that is very much greater than the melting point of LAM. When the shock waves are loaded on the crystal, it will be present in the material only for a few microseconds such that during the very less interaction time, the temperature associated with the shock waves cause local melting in the crystal and immediately solidify. During local melting, diffusion process takes place. Moreover, dynamic recrystallization process takes place concurrently with plastic deformation. The material deforms continuously and every time nucleation of new grains starts and grows within microseconds. The size of the recrystallizing grains decreases as and when the strain rate increases.

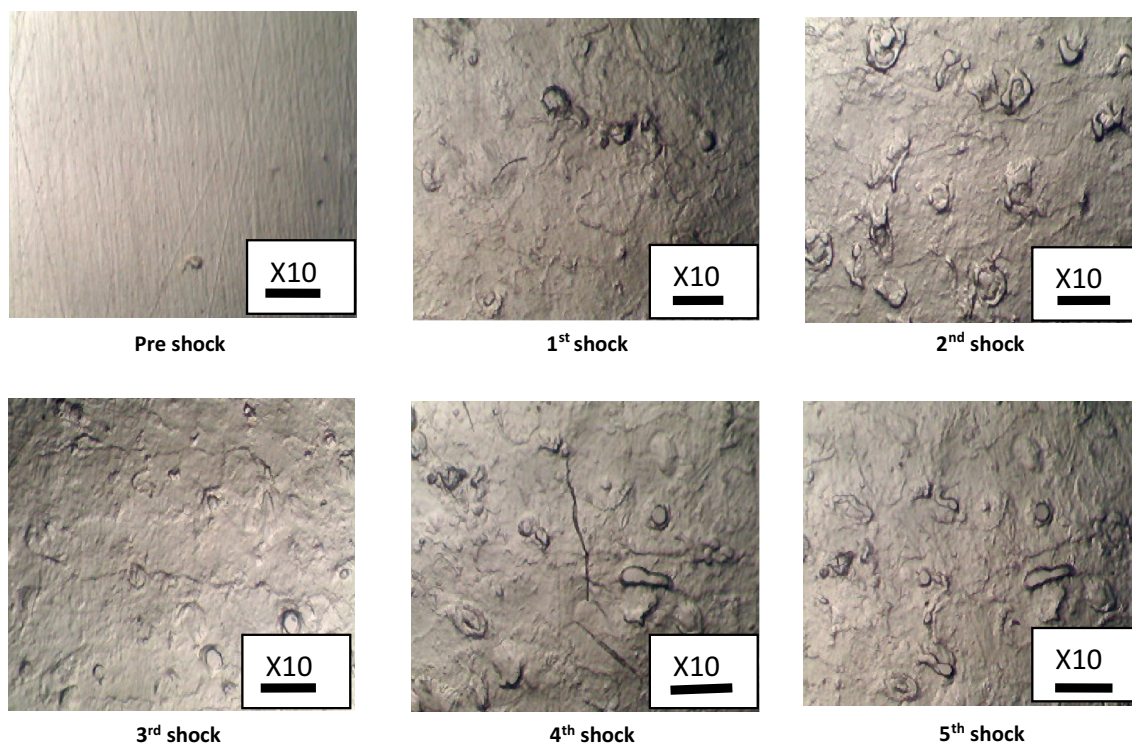


**Figure 1:** Microscopic images of pre- and post-shock-loaded LAM crystal.

In L-alanine maleate, alanine and semimalate ions are arranged as chains parallel to the *b*-axis one after another. Hydrogen bonds link the alanine ions into a straight chain parallel to the *c*-axis. During dynamic recrystallization, diffusion of hydrogen bonds takes place since they are susceptible to high pressure and temperature. Thus, after every shock process, the dynamic recrystallization takes place in the material wherein new grains are formed simultaneously. Hence, for every shock, the surface becomes different. Particularly, the disappearance of cracks takes place by the shock-induced dynamic recrystallization process.

During the process of shock loading, deformation may increase or get reduced depending on the material's nature. In the case of benzil crystal, the transmittance gets increased with the applied shocks, due to shock-induced dynamic recrystallization [18]. But in the present work, the transmittance gets reduced by the shock-induced defects and deformations.

### Structural properties

Structural properties of the LAM crystal before and after shock-loading conditions were analyzed by powder X-ray diffractometer (Bruker D2 Phaser). From the obtained diffraction profiles as reflected in Fig. 2, it is confirmed that the crystal has (002) orientation which belongs to the orthorhombic

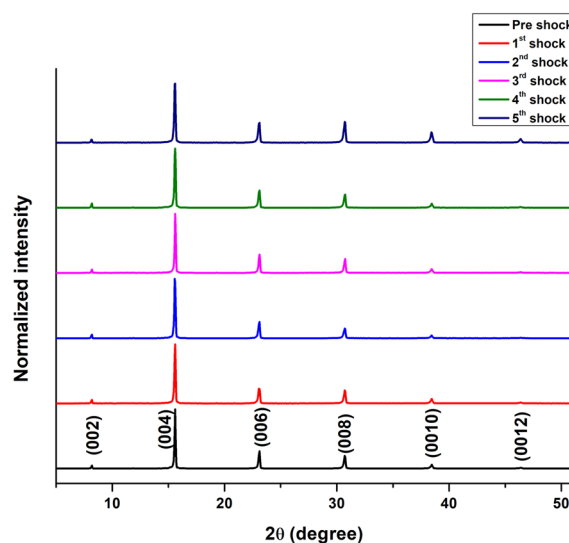


**Figure 2:** X-ray diffraction profile of pre- and post-shock-loaded crystal.

crystal system and  $P2_12_12_1$  space group. Hence, it is found to be in good agreement with Alagar et al. [30]. The pre shock-loaded crystal has five diffraction peaks such as (002), (004), (006), (008), (0010) and (0012) among which (004) peak has the maximum intensity. The presence of the higher-order peaks indicates the high degree of crystallinity of the grown crystal. The post-shocked crystal also shows the same

diffraction peaks as that of the pre-shocked crystal. Since the crystal is grown unidirectionally along the (001) direction, barring this, all the other planes are suppressed, during shock-induced dynamic recrystallization, and also, it took the same direction to recrystallize.

It is clearly observed from Fig. 2 that there is no peak shift or peak disappearance under shock-loaded conditions, but peak broadening as given in Table 1 and peak asymmetry as shown in Fig. 3 are observed in the diffraction peaks. Figure 3 shows zoomed-in version of the (004) diffraction peak.

The shape of the diffraction peak is known to be a function of crystallite size and lattice strain. The diffraction curve of the control crystal shows high peak symmetry whereas in the shocked state, peak asymmetry is observed which is due to shock-induced defects and deformations. From the powder X-ray diffraction study, it is clear that there is no structural phase transition which shows the structural stability of LAM crystal against the impact of shock waves.

### Optical transmittance study

UV-Vis spectrometer (Varian carry 5E Spectrometer) is used to record the optical transmittance of the crystal (thickness 1.5 mm) before and after shock-loading conditions, and the obtained respective spectra are shown in Fig. 4(a) From the observed optical transmittance profile, it is clearly seen that pre- and post-shock-loaded crystal has a wide transmittance window in the visible region. Figure 4(b) shows the shock-transmittance profile of the crystal before and after shock loading wherein pre-shock-loaded crystal has the highest transmittance of 74% at 800 nm.

The optical transmittance of post-shock-loaded crystal has been affected by the impact of shock waves. It has been reported that the optical transmittance of ammonium dihydrogen phosphate [31], magnesium chloride potassium thiocyanate [32], and triglycine sulfate [20] crystals are found to have reduced under the impact of shock waves which typically induce defects and deformations in crystalline materials. On those lines, the optical transmittance of the test crystal gets reduced under

**TABLE 1:** Peak width of diffraction peaks of pre- and post-shock-loaded crystal.

Plane	Peak width (full width at half maximum)					
	Pre shock	1st shock	2nd shock	3rd shock	4th shock	5th shock
(004)	0.122	0.136	0.137	0.119	0.138	0.145
(006)	0.158	0.191	0.173	0.157	0.183	0.198
(008)	0.183	0.197	0.191	0.184	0.195	0.211

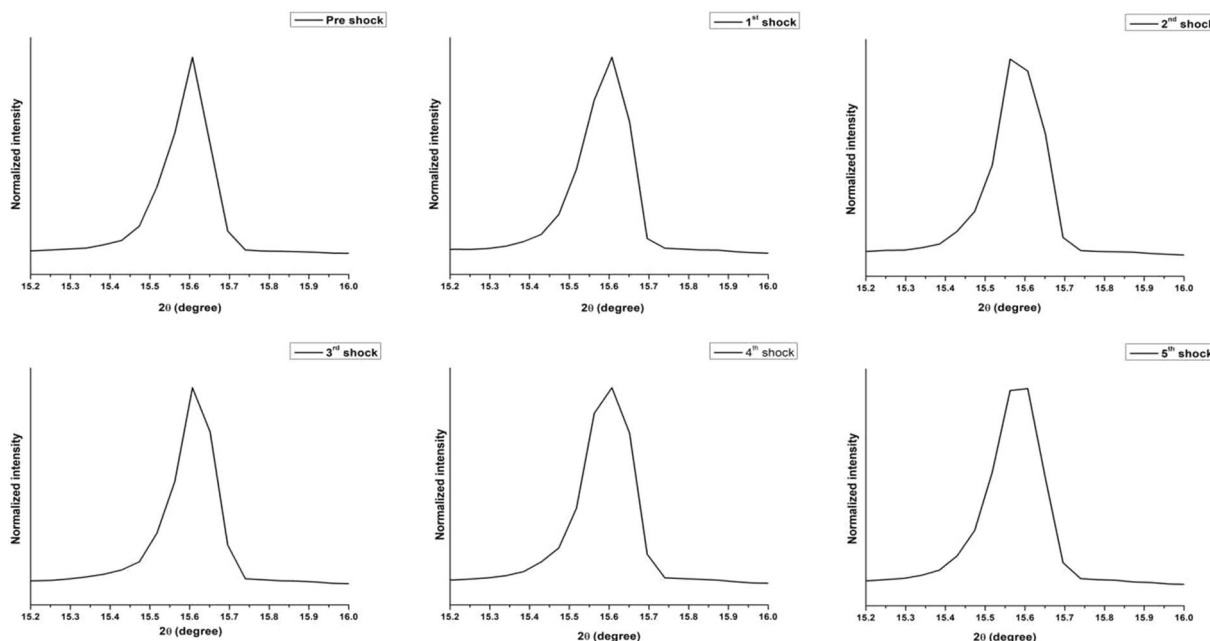


**Figure 3:** Zoomed-in version of the X-ray diffraction profile of pre- and post-shock-loaded crystal in the  $2\theta$  range between  $15.2^\circ$  and  $16^\circ$  corresponding to (004) plane.

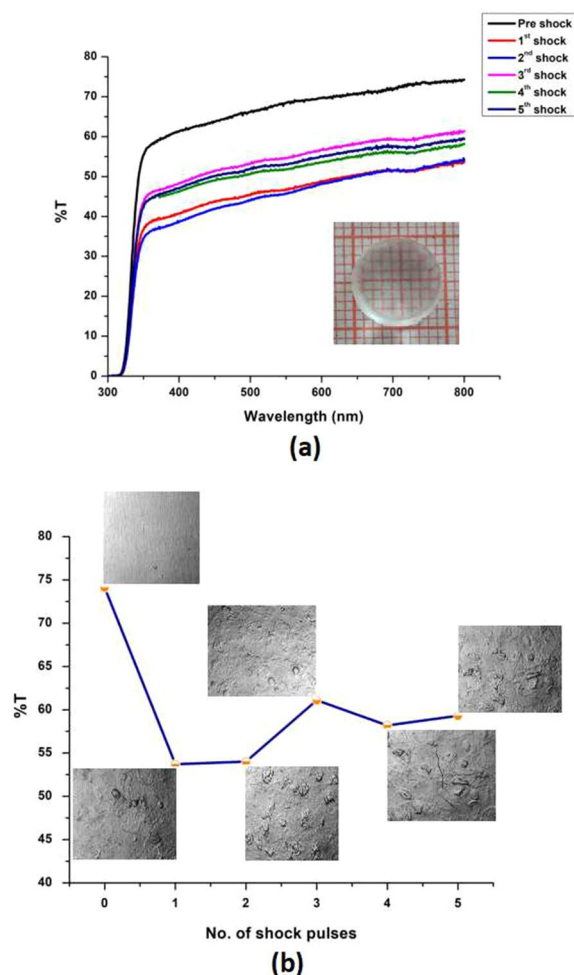


**Figure 4:** (a) Optical transmittance profile and (b) shock-transmittance profile of pre- and post-shock-loaded crystal.

shock-loaded conditions because of the cracks and deformations induced by the shock waves. For the 1<sup>st</sup> and 2<sup>nd</sup> shock-loaded conditions, transmittance of the test crystal is found to have decreased to 53% due to the shock-induced defects and structural disorders, whereas, for the 3<sup>rd</sup> shock-loaded condition, the transmittance has increased to 61% which clearly demonstrates that there is reduced surface defects in the test crystal owing to dynamic recrystallization. Furthermore, after the 4<sup>th</sup> and 5<sup>th</sup> shock-loaded conditions, transmittance of the test crystal is comparatively found to have decreased to 58% and 59%, respectively, which is probably because of the increased surface defects especially the formation of cracks on the surface of the test crystal.

From the obtained transmission spectra, the absorption edge of the test crystal is found to be 330 nm. The optical absorption value of the test crystal has increased under shock-loaded conditions, and it shows the opposite trend of transmittance profile wherein the transmittance of the test crystal is found to have decreased under shock-loaded condition. The increasing

trend of absorption under shock-loaded conditions may be due to the cracks, voids, and disorders induced by the shock impact. However, no change is observed in the absorption edge of the test crystal under shock-loaded conditions, which shows the electronic band stability of the crystal. The absorption coefficient of the material is used to calculate the optical band gap energy of the material which plays an important role in device applications. Note that the optical band gap energy of triglycine sulfate crystal [20] is reduced by shock waves, whereas optical band gap energy of benzil crystal [18] shows an increasing trend with the number of applied shock pulses. Moreover, there is no change observed in the absorption edge as well as optical band gap energy of copper sulfate crystals [19] even after the exposure of 7 shock pulses.

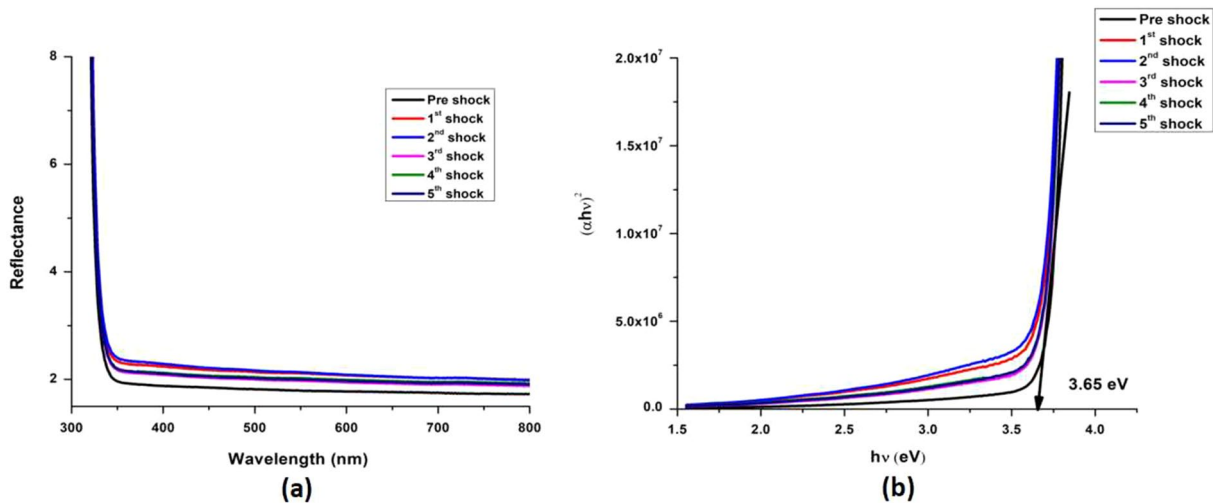
The reflectance of the control and shock-loaded LAM crystal is plotted against wavelength as shown in Fig. 5(a). The reflectance of the control crystal shows less value when compared to the shocked conditions, which clearly shows more light gets reflected by the shock-induced surface defects.

Figure 5(b) shows the optical band gap energy profile of the pre- and post-shock-loaded crystal which is formulated from the Tauc relation. It is found that the band gap energy of the control crystal is 3.65 eV which is in good agreement with the reported values. After shock-loaded conditions, the band gap value remains the same.

### Dielectric properties

The dielectric studies of the LAM crystal before and after shock-loading conditions were undertaken by employing PSM 1735 LCR meter-impedance analyzer. A well-polished LAM crystal of 10.7 mm diameter and 1.9 mm thickness has been fixed between two copper electrodes such that various dielectric parameters were recorded in the frequency range of 1 Hz to 1 MHz at ambient temperature. The dielectric constant, dielectric loss, real and imaginary parts of the impedance, and real and imaginary parts of the permittivity have been calculated for the LAM crystal before and after shock-loading conditions.

Figure 6(a) and (b) displays the respective values of dielectric constant as well as dielectric loss of pre- and 1–5 shock-loaded crystals with respect to frequency. The dielectric constant and dielectric loss of the LAM crystal resembles the behavior of a typical dielectric material. The high value of dielectric constant is identified in the low-frequency region because of the combined contribution of different types of polarization such as ionic, electronic, orientation, and space charge polarization. When the frequency is increased, the electric dipoles are not able to align with the applied field; thereby, the dielectric constant becomes low for the crystal. From Fig. 6(a), it is clear that the dielectric constant decreases on increasing the frequency which is associated to the space



**Figure 5:** (a) Reflectance and (b) optical band gap energy profile of pre and post shock-loaded crystal.

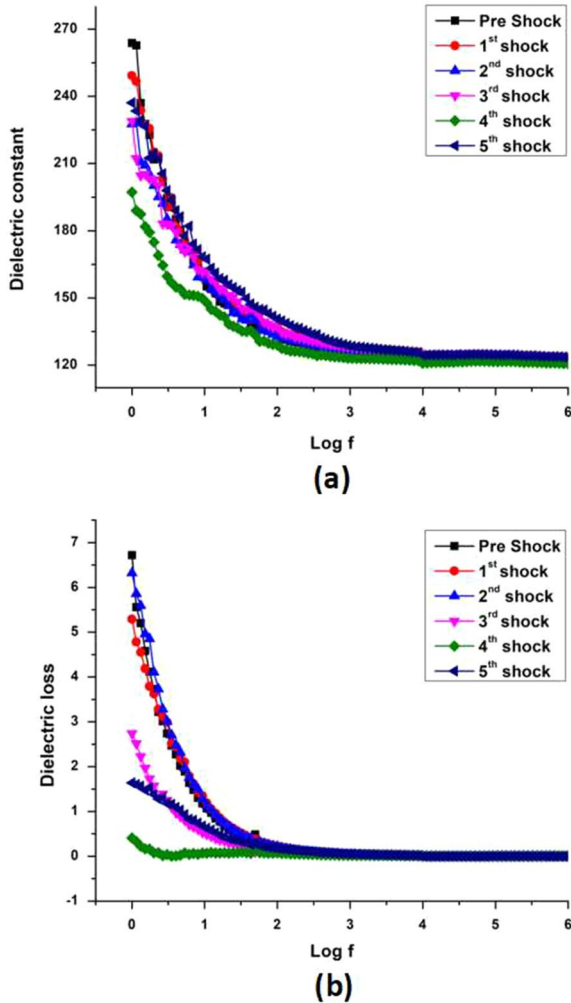


**Figure 6:** (a) Variation of dielectric constant and (b) variation of dielectric loss of pre- and post-shock-loaded crystal with respect to frequency.

charge polarization mechanism arising out of the molecular dipoles near the grain boundary interfaces and it depends upon the measure of perfection of the crystal [8].

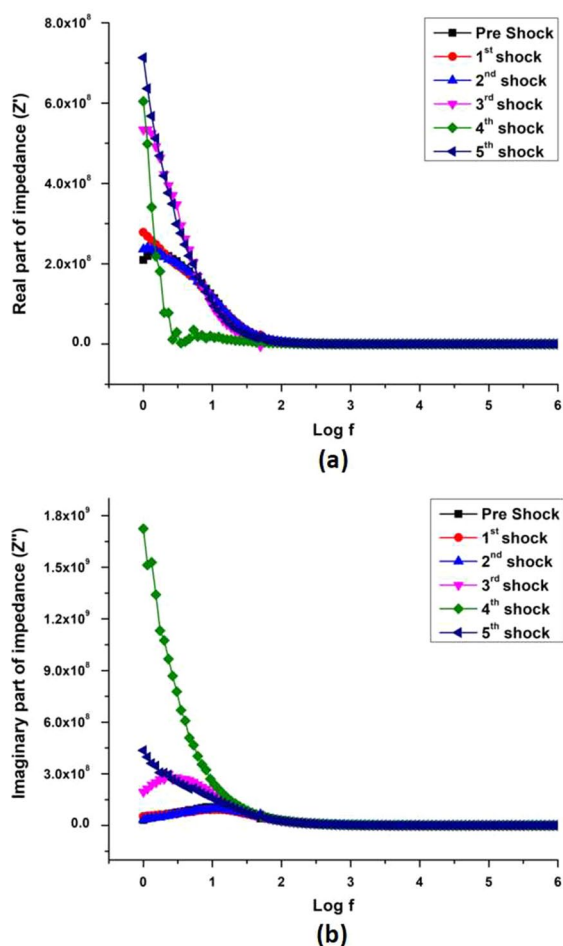
At shocked conditions, a decreasing trend is observed for the dielectric constant in comparison with the pre-shock-loaded crystal. The shock-induced defects are the main reason for the observed decrease in the dielectric constant since the degree of crystallinity plays a prominent role in the dielectric constant of the material [33, 34]. The pre-shocked crystal has high degree of crystallinity; hence, the resistance of the material is less such that the electric dipoles are easily aligned well with the applied electric field. Because of the increased defects and deformations of the test crystal after shocked conditions, the number of grains may increase and grain boundaries such that the resistance of the material increases. Hence, it is difficult for the dipoles to align with the applied field, which leads to a decrease in the dielectric constant. The dielectric constant of the material is directly proportional to its capacitance. The pre-shocked LAM shows higher dielectric constant in comparison with the shocked conditions which is due to the influence of the reduced polarization. It is reported that dielectric constant of KDP crystal is reduced because of the enforced increase in non-90° domain walls under shocked conditions [35], whereas ammonium dihydrogen phosphate (ADP) shows an increase in the number of dipoles under shocked conditions [36].

Figure 6(b) shows that the dielectric loss of the pre- and post-shock-loaded crystal which follow the same behavior as that of the dielectric constant whereby high dielectric loss is observed in the low-frequency region, whereas in the

high-frequency region, it becomes nearly zero. Under shock-loaded conditions, the dielectric loss of the crystal is found to have reduced. The NLO crystal has the required low dielectric constant and dielectric loss so that it is a potential prospect for microelectronic industrial applications [37].

The real and imaginary parts of impedance and the real and imaginary parts of permittivity of LAM crystal before and after shock-loading conditions are calculated using the standard equations [38, 39]. Figure 7(a) and (b) provides the significant values of  $Z'$  and  $Z''$  against frequency, which is found to be maximum in the lower-frequency region whereas on the decreasing mode with the increasing frequency and eventually reaches the value zero for both the pre- and post-shock-loaded crystal. From the observed data, it is evident that the values of  $Z'$  and  $Z''$  are increased under shocked conditions.

Figure 8(a) and (b) portrays the variation of real and imaginary parts of permittivity with respect to the applied electric field while the crystal under the increasing number of shock pulses. It could be authenticated that the control crystal



**Figure 7:** (a) Variation of real part of impedance and (b) variation of imaginary part of impedance of pre- and post-shock-loaded crystal with respect to frequency.

has the maximum value of real and imaginary permittivity in comparison with the shocked crystal. The observed decrease in the values of permittivity under shocked conditions shows that the net polarization of the dipoles is affected by the shock impact.

Figure 8(c) shows the complex impedance plot of the control and shock-loaded LAM crystal. The plot consists of semicircular arcs of which the respective center positions are identified to have deviated from the axis under shocked conditions. The shock-loaded crystal displays higher radius of curvature than the control and especially, the curve for the 4th shocked condition shows the highest value of radius. It is obvious that the electrical resistance of the crystal increases under shocked conditions due to the shock-induced defects and distortions.

## Conclusion

LAM crystals were grown by Sankaranarayanan–Ramasamy method. The present study explores on the impact of shock waves on morphological, structural, optical and dielectric properties of the LAM crystals. Optical micrographs show that the surface of the test crystal is affected by the cracks and defects formed because of shock wave impact. X-ray diffraction studies confirm that there is not any form of the structural phase transition caused by the impact of shock waves which authenticates the structural stability of the test crystal. Optical transmittance of the test crystal is reduced to a certain extent by the surface defects created by the impact of shock waves, but the absorption edge and optical band gap energy are not altered. From the dielectric study, it could be authenticated that the dielectric constant and dielectric loss of the crystal are reduced under shocked conditions which makes it a suitable material for the microelectronic applications. Eventually, it could be concluded that LAM crystal exhibits considerable structural stability and it possesses low dielectric constant against the impact of shock waves such that it could be a suitable material for the applications of microelectronic and optoelectronic devices which work under high-pressure and temperature conditions.

## Experimental section

### Growth of L-alaninium maleate crystal

L-Alanine and maleic acid were taken in 1:1 stoichiometric ratio to synthesize LAM. The saturated solution was prepared at room temperature by dissolving the calculated amount of the respective salts in double-distilled water. The prepared saturated solution was kept in a dust-free environment for slow evaporation at room temperature. After two weeks of time, transparent seed crystals were obtained. A good-quality seed crystal was chosen for the growth under SR method [40] which is used for the unidirectional growth of crystal. LAM crystal is grown along (002)

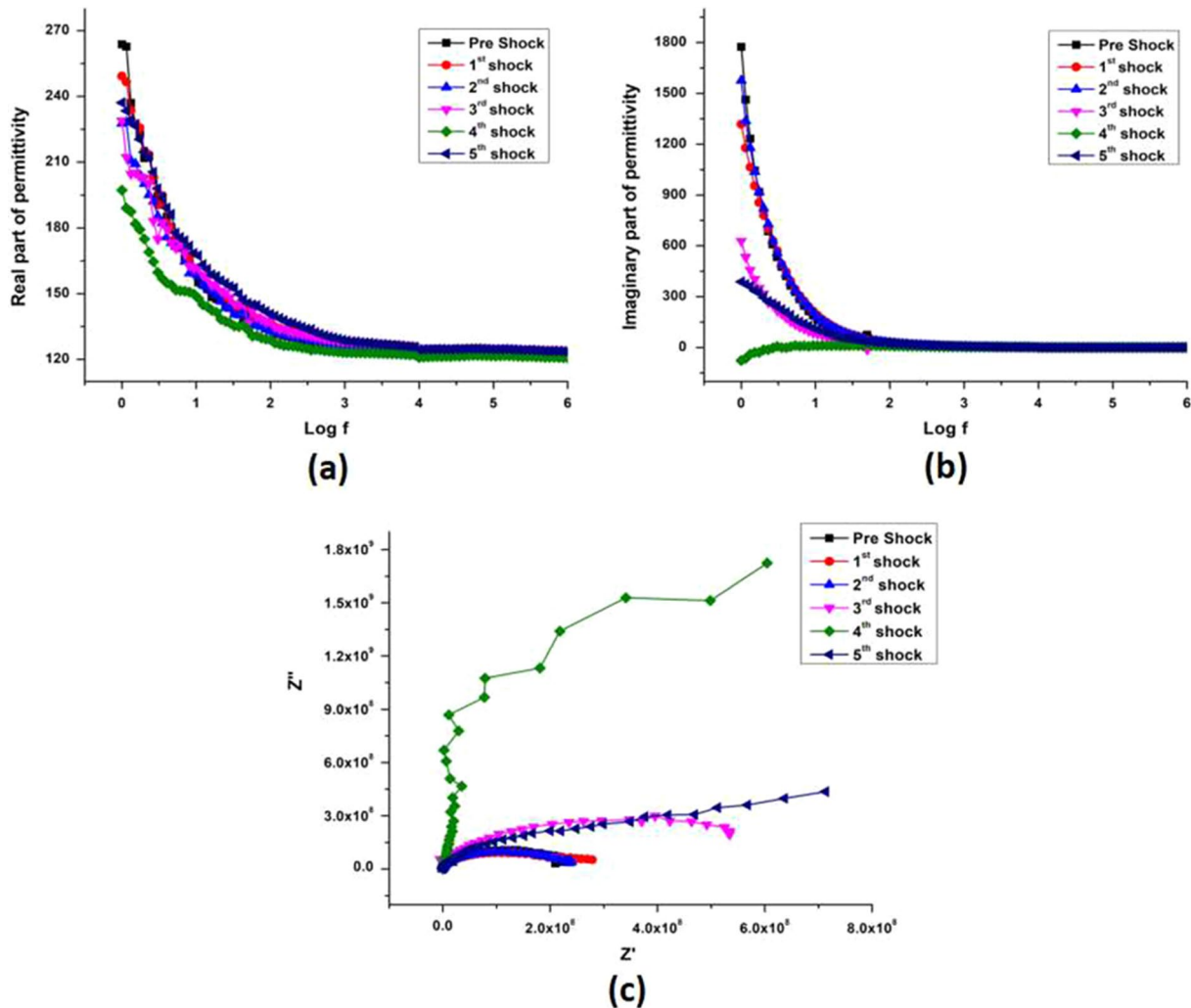


**Figure 8:** (a) Variation of real part of permittivity, (b) variation of imaginary part of permittivity and (c) complex impedance plot of pre- and post-shock-loaded crystal with respect to frequency.

direction by using modified SR method. The seed crystal of good quality that was grown by slow evaporation solution growth method is fixed at the bottom of the ampoule which is filled by the saturated solution of LAM. The ampoule is kept inside the water bath. Two different temperatures are maintained, i.e., one at the top and the other at the bottom of the ampoule. In this setup, a heater coil is fixed near the neck of the ampoule wherein the temperature is controlled by a temperature controller. The temperature near the neck of the ampoule is maintained at 40 °C and the lower end is maintained at room temperature. Because of the temperature gradient existing in the water bath, solution near the heater coil gets evaporated fast when compared with the lower end which leads to concentration gradient in the ampoule. So, the solute in the top end will be attracted to the lower end because of the gravitational force such that it will move towards

seed crystal where nucleation starts at the arrival of the solute and seed crystal starts growing along the fixed (002) direction. After a few weeks, crystal has grown to 5.4 cm length as shown in Fig. 9(a). Utmost care has been taken in cutting and polishing the test crystal. The grown crystal has been cut into thin slices by using a very fine blade and polished by emery sheet of number 1000–3000 until a smooth surface is obtained as shown in Fig. 9(b) and (c).

### Shock wave loading experiment

The indigenously developed semi-automated Reddy tube has been used for the present study whose schematic diagram is shown in Fig. 10.



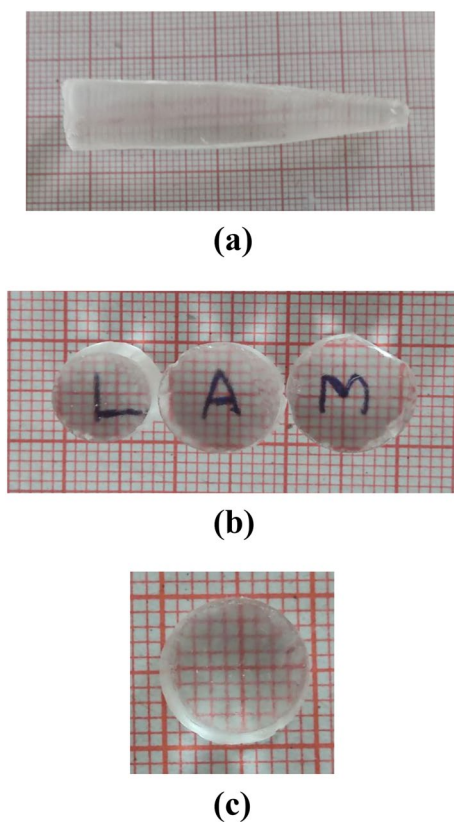


**Figure 9:** Photograph LAM crystal (a) as-grown crystal by SR method, (b), (c) photographs of the cut and polished crystals.

The shock tube consists of three sections named as driver section (high-pressure region), driven section wherein shock waves are generated and diaphragm section which connects driver and driven sections. An 80 GSM paper is used as the diaphragm. The pressure inside the driver section gets increased by the incoming compressed air. At a certain pressure, the diaphragm gets ruptured and shock waves are generated in the driven section, and thereafter, the shock waves are allowed to strike on the test crystal kept in the sample holder. Two pressure sensors which are placed at a distance of 1.8 m apart in the driven section will record the signal in a time scale using *Sound forge* software. This time delay is used to calculate the Mach number of shock waves [41]. The Rankine–Hugoniot equations are used to calculate the pressure and temperature associated with the generated shock waves [42].

Shock waves of 1.7 Mach number that are associated with the transitory pressure of 1.048 MPa and temperature of 644 K have been used for the present study. The grown crystal has been sliced into number of pieces of same magnitude and polished. One of the high-quality cut and polished LAM crystal along the (002) plane possessing 10 mm diameter and 1.5 mm thickness has been chosen and subjected to 5 shock pulses one by one in the sequential order. After every shock, the test crystal has been analyzed by optical microscopy, XRD, UV–Vis spectroscopy and impedance spectroscopy.

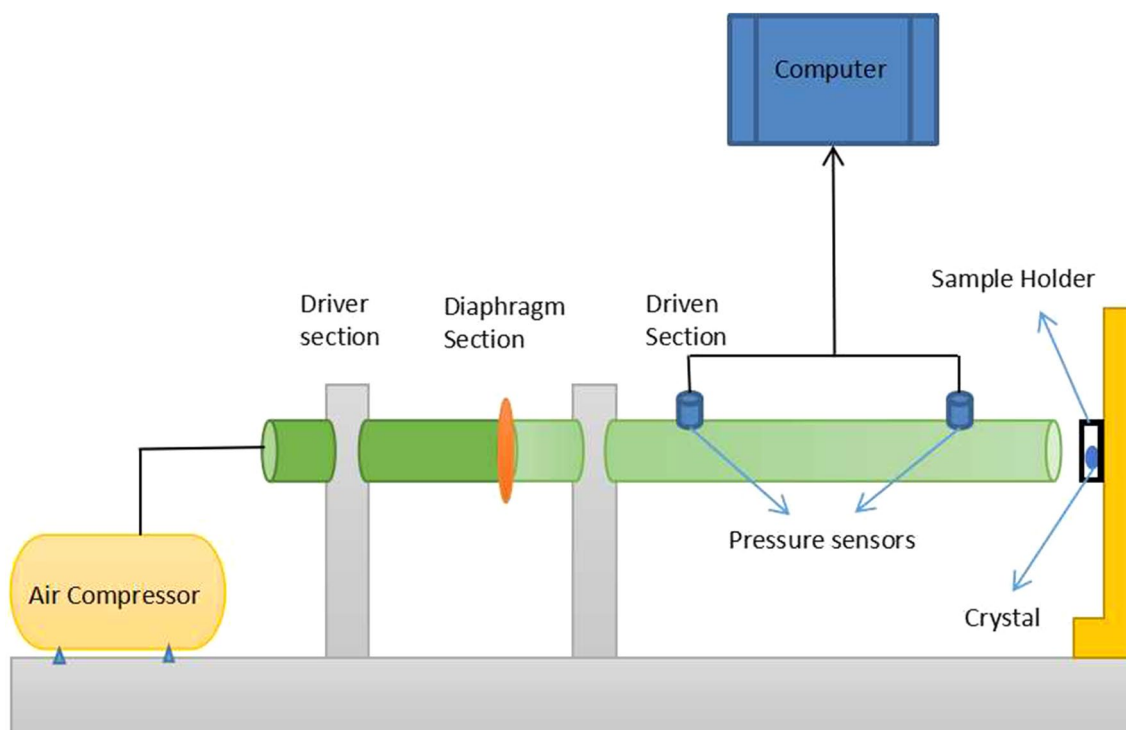


**Figure 10:** Schematic diagram of semi-automated Reddy tube.

## Author contributions

All authors contributed to the study conception and design. Material preparation, data collection, and analysis were performed by [MD], [SSJD], and [SAMBD]. The first draft of the manuscript was written by [MD] and all the authors commented on previous versions of the manuscript. All the authors read and approved the final manuscript.

## Funding

The authors thank the Management of Sacred Heart College for the financial support through Fr.Carreno Research Grant (SHC/Fr. Carreno Research Grant/2022/01) and Don Bosco Research Grant (SHC/DB Grant/2021/01).

## Data availability

The datasets generated and analyzed during the current study are available from the corresponding author on request.

## Code availability

Not applicable.

## Declarations

**Conflict of interest** The authors have no relevant financial or non-financial interests to disclose.

## References

- B.A. Zakharov, E.V. Boldyreva, *Acta Crystallogr. B* **69**, 271–280 (2013). <https://doi.org/10.1107/S2052519213011676>
- A. Dawson, D.R. Allan, S.A. Belmonte, S.J. Clark, W.I.F. David, P.A. McGregor, S. Parsons, C.R. Pulham, L. Sawyer, *Cryst. Growth Des.* **5**, 1415–1427 (2005). <https://doi.org/10.1021/cg049716m>
- V.S. Minkov, E.V. Boldyreva, T.N. Drebushchak, C.H. Görbitz, *CrystEngComm* **14**, 5943–5954 (2012). <https://doi.org/10.1039/C2CE25241D>
- N.A. Tumanov, E.V. Boldyreva, *Acta Crystallogr. B* **68**, 412–423 (2012). <https://doi.org/10.1107/S0108768112028972>
- N.P. Funnell, W.G. Marshall, S. Parsons, *CrystEngComm* **13**, 5841–5848 (2011). <https://doi.org/10.1039/C1CE05487B>
- D. Shanthi, P. Selvarajan, S. Perumal, *Mater. Today Proc.* **2**, 943–948 (2015). <https://doi.org/10.1016/j.matpr.2015.06.013>
- D.A. Fentaw, M.E. Peter, T. Abza, *J. Cryst. Growth* **522**, 1–4 (2019). <https://doi.org/10.1016/j.jcrysgro.2019.06.002>
- L.R. Nirmala, J.T.J. Prakash, *Acta A Mol. Biomol.Spectrosc.* **115**, 778–782 (2013). <https://doi.org/10.1016/j.saa.2013.06.100>
- N. Vijayan, G. Bhagavannarayana, K.K. Maurya, S.N. Sharma, R. Gopalakrishnan, Jayabharathi, P. Ramasamy, *Optik* **123**, 604–608 (2012). <https://doi.org/10.1016/j.ijleo.2011.06.002>
- D. Balasubramanian, R. Jayavel, P. Murugakoothan, *Nat. Sci.* **1**, 216–221 (2009). <https://doi.org/10.4236/ns.2009.13029>
- K. Seethalakshmi, S.K. Mohan, *Asian J. Appl. Sci.* **9**, 23–29 (2016). <https://doi.org/10.3923/ajaps.2016.23.29>
- S.A. Martin Britto Dhas, E. Ramachandran, P. Raji, K. Ramachandran, S. Natarajan, *Cryst. Res. Technol.* **42**, 601–606 (2007). <https://doi.org/10.1002/crat.200610870>
- K. Vasantha, S. Dhanuskodi, *J. Cryst. Growth* **263**, 466–472 (2004). <https://doi.org/10.1016/j.jcrysgro.2003.10.096>
- U. Charoen-In, P. Ramasamy, P. Manyum, *J. Cryst. Growth* **312**, 2369–2375 (2010). <https://doi.org/10.1016/j.jcrysgro.2010.05.027>
- K. Senthil Kannan, B. Kaleemullah Khan, H.A. Jaffar Ali, V.K. Ponnusamy, N.M. Govindan, *Mater. Today Proc.* **33**, 2779–2781 (2020). <https://doi.org/10.1016/j.matpr.2020.02.133>
- G.T. Gray III, Influence of shock-wave deformation on the structure/property behavior of materials, in *High-Pressure Shock Compression of Solids*, ed. by J.R. Asay et al. (Springer, New York, 1993). [https://doi.org/10.1007/978-1-4612-0911-9\\_6](https://doi.org/10.1007/978-1-4612-0911-9_6)
- S.C. Gupta, K.D. Joshi, S. Banerjee, Materials under shock waves, in *Materials Under Extreme Conditions*, ed. by A.K. Tyagi, S. Banerjee (Elsevier, Amsterdam, 2017), pp. 49–89. <https://doi.org/10.1016/B978-0-12-801300-7.00002-4>
- A. Sivakumar, A. Saranraj, S. Sahaya Jude Dhas, S.A. Martin Britto Dhas, *Cryst. Mater. Res. Express* **6**, 046205 (2019). <https://doi.org/10.1088/2053-1591/aafb47>
- A. Sivakumar, M. Sarumathi, S. Sahaya Jude Dhas, S.A. Martin Britto Dhas, *J. Mater. Res.* **35**, 391–400 (2020). <https://doi.org/10.1557/jmr.2019.383>
- A. Sivakumar, A. Saranraj, S. Sahaya Jude Dhas, M. Jose, S.A. Martin Britto Dhas, *Opt. Eng.* **58**, 077104 (2019). <https://doi.org/10.1117/1.OE.58.7.077104>
- A. Sivakumar, S. Sahaya Jude Dhas, S. Balachandar, S.A. Martin Britto Dhas, *J. Electron. Mater.* **48**, 7868–7873 (2019). <https://doi.org/10.1007/s11664-019-07605-9>
- P.A. Urtiew, *J. Appl. Phys.* **45**, 3490 (1974). <https://doi.org/10.1063/1.1663807>
- T. Mashimo, K. Nakamura, K. Tsumoto, Y. Zhang, S. Ando, H. Tonda, *J. Phys. Condens. Matter* **14**, 10783 (2002). <https://doi.org/10.1088/0953-8984/14/44/377>
- K.N. Hemmi, Z.A. Dreger, Y.M. Gupta, *J. Phys. Chem. C* **112**, 7761–7766 (2008). <https://doi.org/10.1021/jp801695x>
- S.V. Singh, J. Vishakantaiiah, J.K. Meka, V. Sivaprasasam, V. Chandrasekaran, R. Thombre, V. Thiruvengatam, A. Mallya, B.N. Rajasekhar, M. Muruganatham, A. Datey, H. Hill, A. Bhardwaj, G. Jagadeesh, K.P.J. Reddy, N.J. Mason, B. Sivaraman, *Molecules* **25**, 5634 (2020). <https://doi.org/10.3390/molecules25235634>
- A. Sivakumar, A. Saranraj, S. Sahaya Jude Dhas, A.I. Almansour, R. Suresh Kumar, N. Arumugam, K. Perumal, S.A. Martin Britto Dhas, *J. Phys. Chem. C* **125**, 25217–25226 (2021). <https://doi.org/10.1021/acs.jpcc.1c07015>

27. A. Sivakumar, S. Sahaya Jude Dhas, P. Sivaprakash, S. Prabhu, K. Moovendaran, A. Murugeswari, S. Arumugam, S.A. Martin Britto Dhas, *J. Mol. Struct.* **1271**, 134033 (2023). <https://doi.org/10.1016/j.molstruc.2022.134033>
28. Yu.I. Meshcheryakov, A.K. Divakov, S.A. Atroshenko, N.S. Naumova, *Tech. Phys. Lett.* **36**, 1125–1128 (2010). <https://doi.org/10.1134/S1063785010120187>
29. S. Atroshenko, *AIP Conf. Proc.* **1748**, 030005 (2016). <https://doi.org/10.1063/1.4954351>
30. M. Alagar, R.V. Krishnakumar, M.S. Nandhini, S. Natarajan, *Acta Crystallogr.* **E57**, 0855–0857 (2001). <https://doi.org/10.1107/S1600536801013149>
31. A. Sivakumar, A. Saranraj, S. Sahaya Jude Dhas, M. Jose, K. Kamala Bharathi, S.A. Martin Britto Dhas, *Opt. Eng.* **58**, 107101 (2019). <https://doi.org/10.1117/1.OE.58.10.107101>
32. K. Showrilu, C. Jyothirmai, A. Sirisha, A. Sivakumar, S. Sahaya Jude Dhas, S.A. Martin Britto Dhas, *J. Mater. Sci. Mater. Electron.* **32**, 3903–3911 (2021). <https://doi.org/10.1007/s10854-020-05133-5>
33. E.S. Kim, C.J. Jeon, *IEEE Trans. Ultrason.* **58**, 1939–1946 (2011). <https://doi.org/10.1109/TUFFC.2011.2034>
34. Kurnia, Heriansyah, E. Suharyadi, *IOP Conf. Ser. Mater. Sci. Eng.* **202**, 012046 (2017). <https://doi.org/10.1088/1757-899X/202/1/012046>
35. A. Sivakumar, M. Manivannan, S. Sahaya Jude Dhas, J. Kalyana Sundar, M. Jose, S.A. Martin Britto Dhas, *Mater. Res. Express* **6**, 086303 (2019). <https://doi.org/10.1088/2053-1591/ab1c96>
36. A. Sivakumar, S. Sahaya Jude Dhas, S. Balachandar, S.A. Martin Britto Dhas, *Z. Kristall Cryst. Mater.* **234**, 557–567 (2019). <https://doi.org/10.1515/zkri-2018-2159>
37. M.R. Baklanov, K. Maex, *Philos. Trans. R. Soc. A* **364**, 201–215 (2006). <https://doi.org/10.1098/rsta.2005.1679>
38. M.H. Al-Saleh, H.K. Al-Anid, Y.A. Husain, H.M. El-Ghanem, S. Abdul Jawad, *J. Phys. D Appl. Phys.* **46**, 385305–385315 (2013). <https://doi.org/10.1088/0022-3727/46/38/385305>
39. M. Kumar, N. Srivastava, *J. Non-Cryst. Solids* **389**, 28 (2014). <https://doi.org/10.1016/j.jnoncrysol.2014.02.002>
40. K. Sankaranarayanan, *J. Cryst. Growth* **284**, 203–208 (2005). <https://doi.org/10.1016/j.jcrysgro.2005.07.019>
41. A. Sivakumar, S. Balachandar, S.A. Martin Britto Dhas, *Hum. Factors Mech. Eng. Def. Saf.* **4**, 3 (2020). <https://doi.org/10.1007/s41314-019-0033-5>
42. E.F. Greene, *J. Chem. Educ.* **41**(2), 114 (1964). <https://doi.org/10.1021/ed041p114.3>

**Publisher's Note** Springer Nature remains neutral with regard to jurisdictional claims in published maps and institutional affiliations.

Springer Nature or its licensor (e.g. a society or other partner) holds exclusive rights to this article under a publishing agreement with the author(s) or other rightsholder(s); author self-archiving of the accepted manuscript version of this article is solely governed by the terms of such publishing agreement and applicable law.